Journal of Materials Science Research and Reviews

7(1): 47-59, 2021; Article no.JMSRR.64597

The Stress Field of a Rectangular Dislocation Loop in an Infinite Medium: Analytical Solution with Verification

Luo Li[1] and Tariq A. Khraishi[1*]

[1]Mechanical Engineering Department, University of New Mexico, Albuquerque, New Mexico, USA.

Authors' contributions

This work was carried out in collaboration between both authors. Author LL was responsible for the derivations, verifications and initial paper write-up. Author TAK designed this research and contributed to paper writing and editing. Both authors read and approved the final manuscript.

Article Information

Editor(s):
(1) Dr. Madogni Vianou Irenee, Universite d'Abomey-Calavi (UAC), Benin.
Reviewers:
(1) Wojciech Macek, University of Occupational Safety Management, Poland,
(2) K. Senthil, National Institute of Technology Jalandhar (NITJ), India.
Complete Peer review History: http://www.sdiarticle4.com/review-history/64597

Original Research Article

Received 02 November 2020
Accepted 07 January 2021
Published 25 January 2021

ABSTRACT

The stress field of a rectangular dislocation loop in an isotropic solid, which is in an infinite medium, is obtained here for a Volterra-type dislocation which has three non-zero Burgers vector components. Explicitly, the stress field of the dislocation loop in an infinite isotropic material is developed by integrating the Peach-Koehler equation over a finite rectangular dislocation loop. In this work, analytical/numerical verification of the stress field is demonstrated. To be specific, the verification is carried out to ensure that both the Equilibrium Equations and the Strain Compatibility Equations are satisfied. Moreover, a comparison with the stress field of a rectangular loop summed as four dislocation segments, using the DeVincre formula, is performed. Due to analytical verification, no error was detected in the presented solution. Also, comparing with the DeVincre formula presented identical results, qualitatively and quantitatively.

Keywords: Rectangular dislocation loop; infinite isotropic material; stress field; numerical/analytical verification.

**Corresponding author: Email: khraishi@unm.edu;*

1. INTRODUCTION

A rectangular dislocation loop is a closed loop formed by four linear dislocation segments. Dislocation lines cannot end inside a material. They have to end on free surfaces, grain boundaries, or form a close loop inside a material [1]. In this work, the development of the stress field of a Volterra-type rectangular dislocation loop is focused on.

The stress solution obtained in this paper facilitates in the development of three-dimensional dislocation dynamics codes [2-3]. The 3D discrete dislocation dynamics (DDD) simulation codes are able to capture the collective interaction of a whole population of curved dislocation lines in a mass of crystalline material on a mesoscopic scale, and to predict mechanical macroscopic behavior out of this interaction. In these codes, a contiguous and curved dislocation line in 3D is discretized in one form or another. One approach is to replace the dislocation line with straight finite-length segments of mixed character [3]. Another approach, followed by [4] is to decompose every segment into two perpendicular segments which are a screw segment and an edge segment. The stress field of the original dislocation curve is then approximated by the additive sum (from the principle of linear superposition) of the self-stresses of the segments composing the curve. Formulae for the self-stress of a straight dislocation segment of mixed character has been given by [5], and by [6].

Different kinds of dislocation problems in terms of material type, geometry and size have been investigated for decades. In the early years, research on infinite isotropic materials was focused on by different researchers. Derivations for the displacement, strain and stress fields of infinite screw and edge dislocations in an infinite medium, assuming material isotropy, were provided [6-8]. Moreover, integral equations for finding the displacement field (the Burgers equation) and the stress field (the Peach-Koehler equation) of a closed dislocation loop (of any shape) in an infinite isotropic material have been provided by [6].

Several researchers have studied different kinds of the dislocation loop problems using various techniques. Initially, [9-10] investigated the prismatic circular loop. The circular glide loop was initially investigated by [11-12]. This solution was later corrected in [13-14]. In a more recent study of the displacement and stress fields of glide and prismatic circular dislocation loops, [15-16] corrected some earlier work. The displacement field, including the solid angle term, of a rectangular dislocation loop of the Volterra type in an infinite medium was developed by [17]. One utility for dislocation loops is its use in the “collocation point” method used to solve traction-free surface problems simulated with the 3-D DDD method via a surface mesh of dislocation loops, see [18-21]. As for circular dislocation loops, they were used for modeling pile-ups around rigid cylindrical particles [22] and for modeling Frank sessile loops which result from irradiation damage in some metals [23-25].

If the Burgers vector is not constant in space, with respect to an inertial coordinate system, but rather varies along the dislocation line, the dislocation is then of the Somigliana type. Work on the ring Somigliana ring dislocation was performed by [26-27] for a radial Burgers vector, and by [28] for a tangential Burgers vector (i.e. a torsional dislocation loop).

In this paper, the stress field of rectangular dislocation loop in an infinite isotropic material is developed by integrating the Peach-Koehler equation over a finite rectangular dislocation loop. Also presented are analytical and numerical verifications of the analytical solution obtained here. Furthermore, a comparison of the stress field developed here and the stress field obtained using the DeVincre’s Formula [5] is performed. The analytical results here add to the knowledge base of solutions for dislocations of different geometries. It has direction applications in Eigenstrain theory/computations [29] and the collocation-point method for capturing the effect of free surfaces on dislocation forces/motion [30].

2. INTEGRATION OF THE PEACH-KOEHLER (PK) EQUATION

The dislocation problem under consideration is shown in Fig. 1. The figure shows a rectangular dislocation loop (also described as a “finite-sized dislocation loop”) in an infinite isotropic medium. This Volterra-type dislocation loop has three Burgers vector components b_x, b_y and b_z, and has a dimension 2*a* in the *x*-direction and a dimension 2*b* in the *y*-direction. The line sense of the dislocation loop is shown by the arrow along the dislocation loop. The goal in this problem is to obtain the stress components for an arbitrary material field point P. Note that in this paper x_1 and *x* are used interchangeably, so are x_2 and *y*, and so are x_3 and z. Analogously for x'_1 and x', and so on.

The PK Equation (1) is an integral equation for the stress field of any curved closed dislocation loop [6]. It is composed of three terms. They are all line integrals and they sum the contributions of infinitesimal line lengths (dl') along the line sense of the loop:

$$\sigma_{\alpha\beta} = -\frac{G}{8\pi}\oint_C b_m\epsilon_{im\alpha}\frac{\partial}{\partial x_i'}\nabla'^2 R dx_\beta' - \frac{G}{8\pi}\oint_C b_m\epsilon_{im\beta}\frac{\partial}{\partial x_i'}\nabla'^2 R dx_\alpha' - \frac{G}{4\pi(1-\upsilon)}\oint_C b_m\epsilon_{imk}(\frac{\partial^3 R}{\partial x_i'\partial x_\alpha'\partial x_\beta'} - \delta_{\alpha\beta}\frac{\partial}{\partial x_i'}\nabla'^2 R)dx_k'; \quad (1)$$

$$\sigma_{\alpha\beta}term1 = -\frac{G}{8\pi}\oint_C b_m\epsilon_{im\alpha}\frac{\partial}{\partial x_i'}\nabla'^2 R dx_\beta'; \quad (2)$$

$$\sigma_{\alpha\beta}term2 = -\frac{G}{8\pi}\oint_C b_m\epsilon_{im\beta}\frac{\partial}{\partial x_i'}\nabla'^2 R dx_\alpha'; \quad (3)$$

$$\sigma_{\alpha\beta}term3 = -\frac{G}{4\pi(1-\upsilon)}\oint_C b_m\epsilon_{imk}(\frac{\partial^3 R}{\partial x_i'\partial x_\alpha'\partial x_\beta'} - \delta_{\alpha\beta}\frac{\partial}{\partial x_i'}\nabla'^2 R)dx_k'; \quad (4)$$

Where $\sigma_{\alpha\beta}$ is the $\alpha\beta^{th}$ component of the stress tensor $\boldsymbol{\sigma}$, b_m is the m^{th} component of the displacement vector $\vec{b} = \mathbf{b} = (b_x, b_y, b_z)$, δ_{ij} is the ij^{th} component of the Kronecker delta, G is the shear modulus, $\in$ is the permutation symbol, ν is Poisson's ratio, $R = \sqrt{(x' - x)^2 + (y' - y)^2 + (z' - z)^2}$ (see Fig. 1) and $\nabla'^2 R = 2/R$.

For integration of the Peach-Koehler Equation, some steps need to be considered for the rectangular loop in Figure 1 which is composed of four numbered segments/sides. First, the elevation of the dislocation loop above the *xy*-plane is fixed in the xyz global coordinate system, which means the value of z' is constant in this case or $dz' = 0$. Second, x' is a constant equal to $+a$ along segment 1, which means $dx' = 0$ along this segment. Analogously, $x' = -a$ and $dx' = 0$ along segment 3, $y' = +b$ and $dy' = 0$ along segment 2, $y' = -b$ and $dy' = 0$ along segment 4.

For the sake of illustration, only the integration for σ_{xz} for a non-zero b_z is shown as an example of the integration of the PK Equation:

$$\sigma_{xz}term1 = -\frac{G}{8\pi}\oint_C b_z\epsilon_{izx}\frac{\partial}{\partial x_i'}\frac{2}{R}dz' = 0 \quad ; (dz' = 0) \quad (5)$$

$$\sigma_{xz}term2 = -\frac{G}{8\pi}\oint_C b_z\epsilon_{izz}\frac{\partial}{\partial x_i'}\frac{2}{R}dx' = 0 \quad ; (\epsilon_{izz} = 0) \quad (6)$$

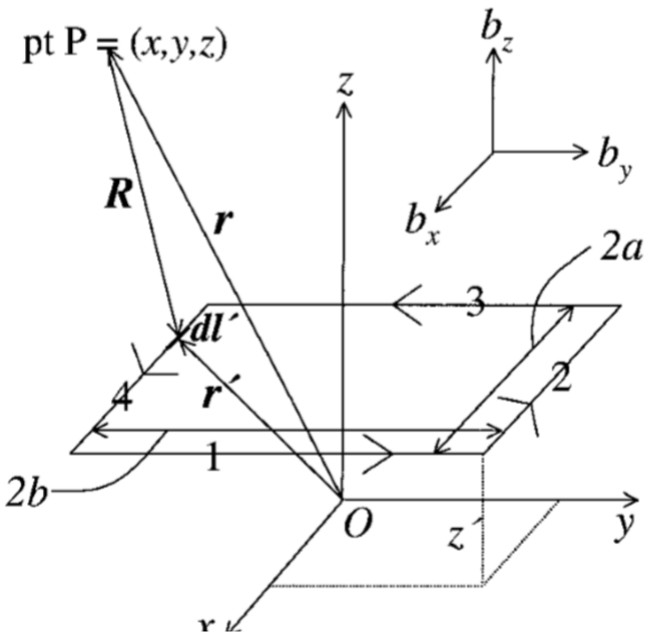

Fig. 1. The geometry of a rectangular dislocation loop in an infinite material. Here $\vec{r}' = r' = (x', y', z')$. The primed quantities belong to a differential length dl' on the dislocation loop

$$\sigma_{xz}term3 = -\frac{G}{4\pi(1-\upsilon)}\oint_C b_z\epsilon_{xzy}\left(\frac{\partial^3 R}{\partial^2 x'\partial z'} - \delta_{xz}\frac{\partial}{\partial x'}\frac{2}{R}\right)dy' - \frac{G}{4\pi(1-\upsilon)}\oint_C b_z\epsilon_{yzx}\left(\frac{\partial^3 R}{\partial y'\partial x'\partial z'} - \delta_{xz}\frac{\partial}{\partial y'}\frac{2}{R}\right)dx' = \frac{G}{4\pi(1-\upsilon)}\oint_C b_z\left(\frac{\partial^3 R}{\partial^2 x'\partial z'}\right)dy' - \frac{G}{4\pi(1-\upsilon)}\oint_C b_z\left(\frac{\partial^3 R}{\partial y'\partial x'\partial z'}\right)dx';\ (\epsilon_{xzy} = -1, \epsilon_{yzx} = 1, \delta_{xz} = 0) \quad (7)$$

Hence,

$$\sigma_{xz} = \sigma_{xz}term1 + \sigma_{xz}term2 + \sigma_{xz}term3 = \frac{G}{4\pi(1-\upsilon)}\oint_C b_z\left(\frac{\partial^3 R}{\partial^2 x'\partial z'}\right)dy' - \frac{G}{4\pi(1-\upsilon)}\oint_C b_z\left(\frac{\partial^3 R}{\partial y'\partial x'\partial z'}\right)dx' = \{\frac{Gb_z}{4\pi(1-\upsilon)}\int_{-b}^{+b}[\left(\frac{\partial^3 R}{\partial^2 x'\partial z'}\right)dy']_{x'=+a}\} + \{\frac{Gb_z}{4\pi(1-\upsilon)}\int_{+b}^{-b}[\left(\frac{\partial^3 R}{\partial^2 x'\partial z'}\right)dy']_{x'=-a}\} - \{\frac{Gb_z}{4\pi(1-\upsilon)}\int_{+a}^{-a}[\left(\frac{\partial^3 R}{\partial y'\partial x'\partial z'}\right)dx']_{y'=+b}\} - \{\frac{Gb_z}{4\pi(1-\upsilon)}\int_{-a}^{+a}[\left(\frac{\partial^3 R}{\partial y'\partial x'\partial z'}\right)dx']_{y'=-b}\}; \quad (8)$$

Let's focus on the integral: $\frac{Gb_z}{4\pi(1-\upsilon)}\int_{-b}^{+b}[\left(\frac{\partial^3 R}{\partial^2 x'\partial z'}\right)dy']_{x'=+a}$. For the integrand $\frac{\partial^3 R}{\partial^2 x'\partial z'}$, it is given by:

$$\frac{\partial^3 R}{\partial^2 x'\partial z'} = \frac{3(-x+x')^2(-z+z')}{((-x+x')^2+(-y+y')^2+(-z+z')^2)^{5/2}} - \frac{-z+z'}{((-x+x')^2+(-y+y')^2+(-z+z')^2)^{3/2}}$$

Hence, the integral $\frac{Gb_z}{4\pi(1-\upsilon)}\int_{-b}^{+b}[\left(\frac{\partial^3 R}{\partial^2 x'\partial z'}\right)dy']_{x'=+a}$ is in actuality composed of two integrals:

$$\frac{Gb_z}{4\pi(1-\upsilon)}\int_{-b}^{+b}[\left(\frac{3(-x+x')^2(-z+z')}{((-x+x')^2+(-y+y')^2+(-z+z')^2)^{5/2}}\right)dy']_{x'=+a}$$

and

$$-\frac{Gb_z}{4\pi(1-\upsilon)}\int_{-b}^{+b}[\left(\frac{-z+z'}{((-x+x')^2+(-y+y')^2+(-z+z')^2)^{3/2}}\right)dy']_{x'=+a}\ .$$

If one is interested in integrating by hand or manually, one can use the integral tables in [31]. We only show how to integrate the second integral here, i.e.

$$-\frac{Gb_z}{4\pi(1-\upsilon)}\int_{-b}^{+b}[\left(\frac{-z+z'}{((-x+x')^2+(-y+y')^2+(-z+z')^2)^{3/2}}\right)dy']_{x'=+a}.$$

According to [31], $\int\frac{dx}{\sqrt{R_1}^3} = \frac{2(2cx+b)}{(4ac-b^2)\sqrt{R_1}}$, (9)

Where $R_1 = a + bx + cx^2$; Note that the integrand $\frac{-z+z'}{((-x+x')^2+(-y+y')^2+(-z+z')^2)^{3/2}}$ can be written as $\frac{-z+z'}{(y'^2-2y'y+y^2+(-x+x')^2+(-z+z')^2)^{3/2}}$.

In this example, $R_1 = y'^2 - 2y'y + y^2 + (-x+x')^2 + (-z+z')^2 = a + by' + cy'^2$, where $a = y^2 + (-x+x')^2 + (-z+z')^2$, $b = -2y$, $c = 1$. According to equation (9),

$$\int\frac{-z+z'}{(y'^2-2y'y+y^2+(-x+x')^2+(-z+z')^2)^{3/2}}dy' = \int\frac{(-z+z')dy'}{\sqrt{R_1}^3} = \frac{2(2cy'+b)(-z+z')}{(4ac-b^2)\sqrt{R_1}} = \frac{2(2y'-2y)(-z+z')}{(4(y^2+(-x+x')^2+(-z+z')^2)-4y^2)\sqrt{y'^2-2y'y+y^2+(-x+x')^2+(-z+z')^2}} = \frac{(y'-y)(-z+z')}{((-x+x')^2+(-z+z')^2)\sqrt{(-y+y')^2+(-x+x')^2+(-z+z')^2}};$$

Hence finally,

$$-\frac{Gb_z}{4\pi(1-\upsilon)}\int_{-b}^{+b}[\left(\frac{-z+z'}{((-y+y')^2+(-x+x')^2+(-z+z')^2)^{3/2}}\right)dy']_{x'=+a} = -\frac{Gb_z}{4\pi(1-\upsilon)}\{\left[\frac{(b-y)(-z+z')}{((-x+a)^2+(-z+z')^2)\sqrt{(-y+b)^2+(-x+a)^2+(-z+z')^2}}\right] - \left[\frac{(-b-y)(-z+z')}{((-x+a)^2+(-z+z')^2)\sqrt{(-y-b)^2+(-x+a)^2+(-z+z')^2}}\right]\}; \quad (10)$$

Moreover, one can also use the mathematical software Mathematica, which has a very strong symbolic engine, to do the integration instead. This provides efficiency and time savings.

3. RESULTS AND DISCUSSION

The stress field terms for a rectangular dislocation loop in an infinite medium were integrated from the PK Equation using the software Mathematica. The full list of results for the stress components, based on the Burgers vector components, are supplied in the appendices. For a loop with more than one, or all three, of the Burgers vector components not being zero, then the stress component is simply the sum, from the principle of superposition, of the results for these different Burgers vector components (as in the appendices). Note that in the appendices, we have replaced the z' in Fig. 1 with *c*.

If one is interested in the strain field terms or components instead, which are not listed here for brevity, these could be obtained from the stresses in the appendices using the inverted Hooke's law for isotropic materials:

$$\epsilon_{ij} = \frac{1}{2G}\left(\sigma_{ij} - \frac{\lambda\delta_{ij}}{2G+3\lambda}\sigma_{kk}\right) \quad (11)$$

Where σ_{kk} is the first invariant of the stress tensor, $\lambda = \frac{E\nu}{(1+\nu)(1-2\nu)}$, $G = \frac{E}{2(1+\nu)}$, and E is Young's modulus.

3.1 Equilibrium Equations Verification

The partial differential equations of static equilibrium in a solid material can be written in indicial notation as:

$$\sigma_{ij,j} = \frac{\partial \sigma_{ij}}{\partial x_j} = 0 \quad (12)$$

If the last equation is expanded on the repeated indices then the resulting three equations are:

$$\frac{\partial \sigma_{xx}}{\partial x} + \frac{\partial \sigma_{xy}}{\partial y} + \frac{\partial \sigma_{xz}}{\partial z} = 0 \quad (13)$$

$$\frac{\partial \sigma_{yx}}{\partial x} + \frac{\partial \sigma_{yy}}{\partial y} + \frac{\partial \sigma_{yz}}{\partial z} = 0 \quad (14)$$

$$\frac{\partial \sigma_{zx}}{\partial x} + \frac{\partial \sigma_{zy}}{\partial y} + \frac{\partial \sigma_{zz}}{\partial z} = 0 \quad (15)$$

This is keeping in mind the symmetry of the stress tensor, i.e. $\sigma_{ij} = \sigma_{ji}$. These equations should be satisfied at every material point of a solid in equilibrium. To verify the developed stress solution $\sigma_{\alpha\beta}$ given by equation (1) and provide in the appendices, one can see if equations (13-15) are identically satisfied either using analytical or numerical methods. For the analytical method, the equations are all reduced to zero by utilizing Mathematica. Similarly if one considers any line in space. For such line, the three equilibrium equations also equate analytically, or exactly, to zero. Hence, analytical verification of the equilibrium equations is feasible.

Alternatively, numerical verifications can also be made by plotting equations (13-15) along any plane in the material to see if the equations show a zero result. Figure (2.1, 2.2, 2.3) shows such plotting for $b_x \neq 0$. The figure shows that the equilibrium equations are satisfied. Note that given the combination of Burgers vector components and equilibrium equations a total of nine plots are minimally generated. For this reason, only three plots for one of the Burgers vector components are shown here for brevity.

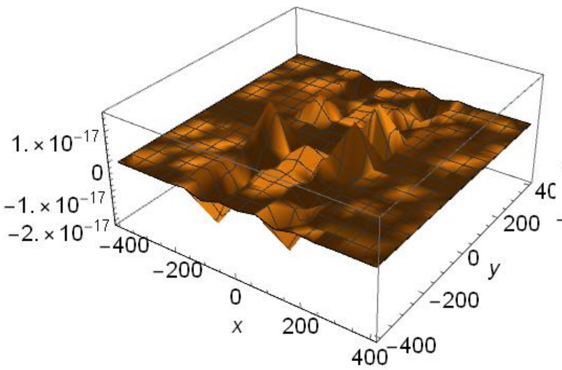

Fig. 2.1. Plot of equation (13)

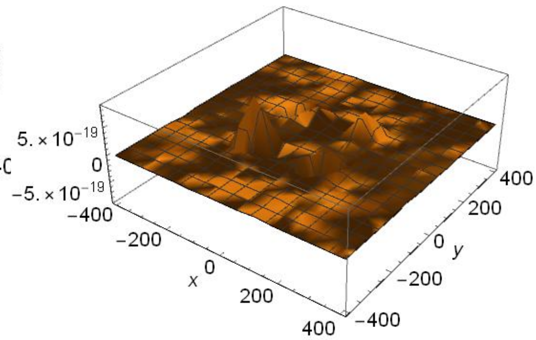

Fig. 2.2. Plot of equation (14)

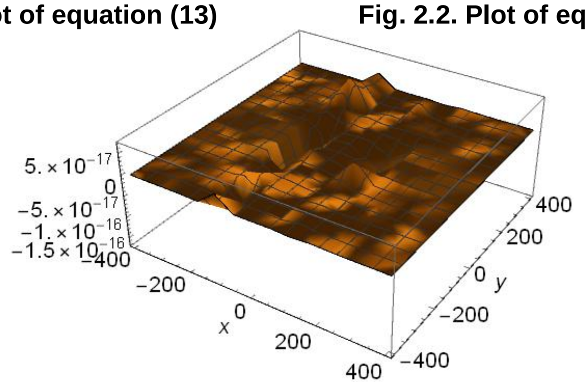

Fig. 2.3. Plot of equation (15). For these plots, the following values were chosen: $a = b = 100b_x$, $c = 10b_x$, $b_y = b_z = 0$, $b_x = 1$, $\nu = 0.3$, $\mu = 100$, $z = 11b_x$ $-4a \leq x \leq 4a$, $-4b \leq y \leq 4b$

3.2 Strain Compatibility Equations Verification

The equations of compatibility can be written in indicial notation as [32]:

$$\epsilon_{ij,kl} - \epsilon_{jl,ik} - \epsilon_{ik,jl} + \epsilon_{kl,ij} = 0 \tag{16}$$

This equation can be expanded over the repeated indices and written explicitly as six different/unique equations:

$$\frac{\partial^2 \epsilon_{xx}}{\partial y^2} + \frac{\partial^2 \epsilon_{yy}}{\partial x^2} = 2\frac{\partial^2 \epsilon_{xy}}{\partial x \partial y} \tag{17}$$

$$\frac{\partial^2 \epsilon_{xx}}{\partial z^2} + \frac{\partial^2 \epsilon_{zz}}{\partial x^2} = 2\frac{\partial^2 \epsilon_{xz}}{\partial x \partial z} \tag{18}$$

$$\frac{\partial^2 \epsilon_{zz}}{\partial y^2} + \frac{\partial^2 \epsilon_{yy}}{\partial z^2} = 2\frac{\partial^2 \epsilon_{zy}}{\partial z \partial y} \tag{19}$$

$$\frac{\partial^2 \epsilon_{xx}}{\partial y \partial z} + \frac{\partial^2 \epsilon_{yz}}{\partial x^2} = \frac{\partial^2 \epsilon_{xz}}{\partial x \partial y} + \frac{\partial^2 \epsilon_{xy}}{\partial x \partial z} \tag{20}$$

$$\frac{\partial^2 \epsilon_{yy}}{\partial x \partial z} + \frac{\partial^2 \epsilon_{xz}}{\partial y^2} = \frac{\partial^2 \epsilon_{xy}}{\partial y \partial z} + \frac{\partial^2 \epsilon_{yz}}{\partial x \partial y} \tag{21}$$

$$\frac{\partial^2 \epsilon_{zz}}{\partial x \partial y} + \frac{\partial^2 \epsilon_{xy}}{\partial z^2} = \frac{\partial^2 \epsilon_{xz}}{\partial y \partial z} + \frac{\partial^2 \epsilon_{yz}}{\partial x \partial z} \tag{22}$$

These equations should be satisfied at every material point of a solid. To verify the developed stress solution, $\boldsymbol{\epsilon}$ (the strain tensor) and its components are given by equation (11). One can then investigate if equations (17-22) are identically zero using either analytical or numerical methods. For the analytical method, the equations are so large that Mathematica is not able to reduce them to exactly 0. However, for any given line in space along the *x*-, *y*- or *z*-directions, Mathematica identically simplifies the compatibility equations to zero. Hence analytical verification of the compatibility equations is possible.

Alternatively, numerical verifications can also be made by plotting equations (17-22) along any plane in the material to see if the equations give a zero result. Figure (3.1, 3.2, 3.3) shows such plotting for b_y ≠ 0. The figure shows that the compatibility equations are satisfied. Note that given the combination of Burgers vector components and compatibility equations a total of eighteen plots are minimally generated. However, only three plots for one of the Burgers vector components are shown here for brevity.

3.3 Comparision with Devincre's Formula

The DeVincre's Formula [5] is an expression for the stress field of a straight or linear dislocation segment of finite length :

$$\sigma_{ij} = \frac{\mu}{\pi Y^2}\Big\{[\boldsymbol{b}'\boldsymbol{Y}\boldsymbol{t}']^s_{ij} - \frac{1}{1-\nu}[\boldsymbol{b}'\boldsymbol{t}'\boldsymbol{Y}]^s_{ij} - \frac{(\boldsymbol{b}',\boldsymbol{Y},\boldsymbol{t}')}{2(1-\nu)}\left[\delta_{ij} + t_i' t_j' + \frac{2}{Y^2}\left[\rho_i Y_j + \rho_j Y_i + \frac{L'}{R} Y_i Y_j\right]\right]\Big\} \tag{23}$$

Where $\boldsymbol{b}'$ is the Burgers vector, $\boldsymbol{b}' = (b_x, b_y, b_z)$, $\boldsymbol{t}'$ is the line sense vector or the line direction, $\boldsymbol{t}' = (t_x, t_y, t_z)$, σ_{ij} is ij^{th} component of the stress tensor, $\boldsymbol{Y} = \boldsymbol{R} + R\boldsymbol{t}'$, $\boldsymbol{R} = ((x'-x),(y'-y),(z'-z))$, $R = \sqrt{(x'-x)^2 + (y'-y)^2 + (z'-z)^2}$, δ_{ij} is the ij^{th} component of the Kronecker delta, μ is shear modulus, ν is Poisson's ratio, $L' = \boldsymbol{R}\cdot\boldsymbol{t}'$, $\boldsymbol{\rho} = \boldsymbol{R} - L'\boldsymbol{t}'$, $(\boldsymbol{b}',\boldsymbol{Y},\boldsymbol{t}') = (\boldsymbol{b}'\times\boldsymbol{Y})\cdot\boldsymbol{t}'$, and $[\boldsymbol{abc}]^s_{ij} = \frac{1}{2}((\boldsymbol{a}\times\boldsymbol{b})_i c_j + (\boldsymbol{a}\times\boldsymbol{b})_j c_i)$. Note that bold lettering represents a vector(s) herein.

In this paper, the rectangular dislocation loop which is composed of four straight dislocation segments (or sides) is focused on here. Hence, the stress field of a rectangular dislocation can be obtained by adding up the contributions of four straight dislocation segments each obtained from the DeVincre's Formula.

To compare with the stress field obtained from the DeVincre's Formula, the following parameters are used for the plots in Figs. 4-9:

$$a = b = 100,\ c = 0,\ \nu = 0.3,\ b_x = b_y = 0;$$
$$b_z = 1;\ y = 0, z = 20b_z,\ -2a \le x \le 2a,$$

The figures show perfect match between the analytical solution in this paper and the solution obtained from utilizing DeVincre's Formula. This provides confidence in the presented analytical stress solution since it is matching the solution of four connected segments. Note that given the combination of Burgers vector components and stress components a total of eighteen plots are minimally generated. However, only six plots for one of the Burgers vector components are shown here for brevity.

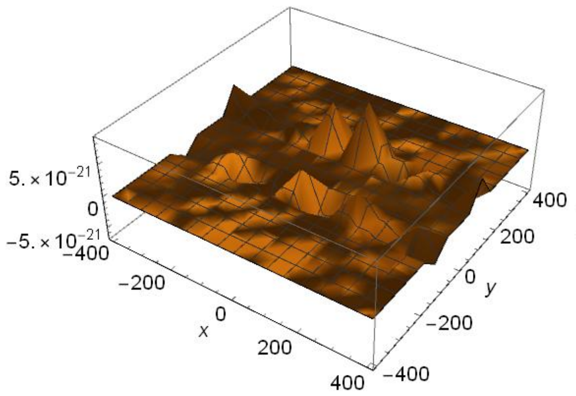

Fig. 3.1. Plot of equation (17)

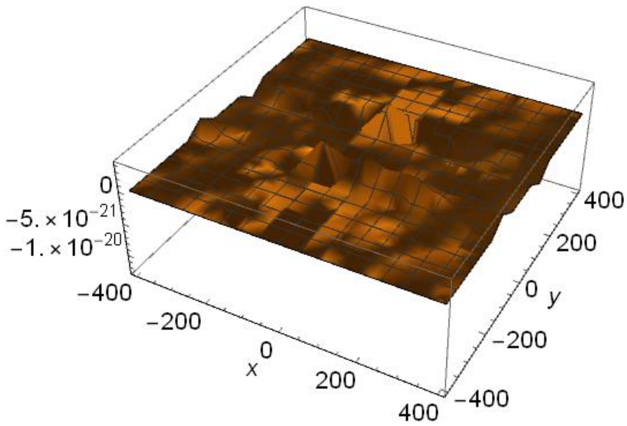

Fig. 3.2. Plot of equation (18)

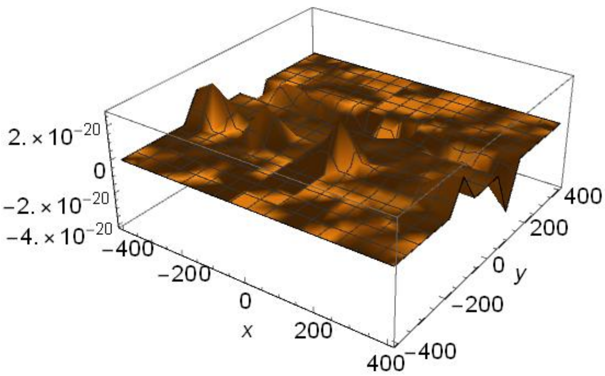

Fig. 3.3. Plot of equation (19). For these plots, the following values were chosen: $a = b = 100b_y$, $c = 10b_y$, $b_x = b_z = 0$, $b_y = 1$, $\nu = 0.3$, $\mu = G = 100$, $z = 11b_y$ $-4a \leq x \leq 4a$, $-4b \leq y \leq 4b$

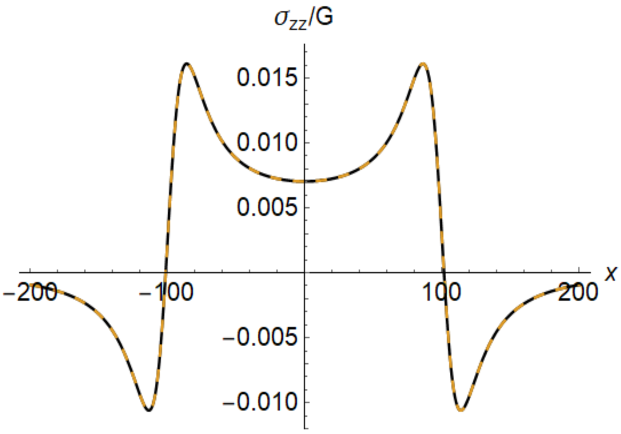

Fig. 4. Comparison of $\frac{\sigma_{zz}}{G}$ analytical solutions in this paper (solid and black line) to the results of DeVincre's Formula (dashed line) along *x*-direction for non-zero b_z

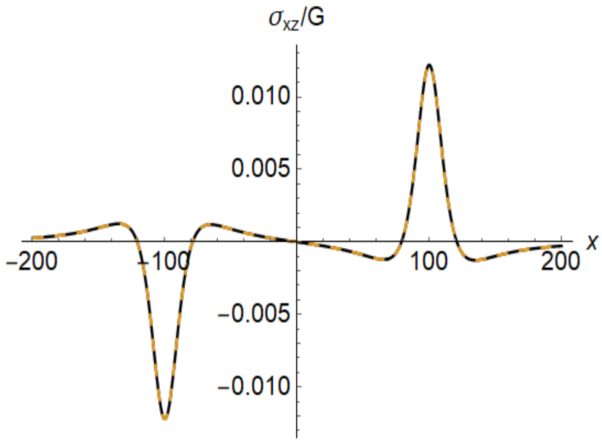

Fig. 5. Comparison of $\frac{\sigma_{xz}}{G}$ analytical solutions in this paper (solid and black line) to the results of Devincre's Formula (dashed line) along *x*-direction for non-zero b_z

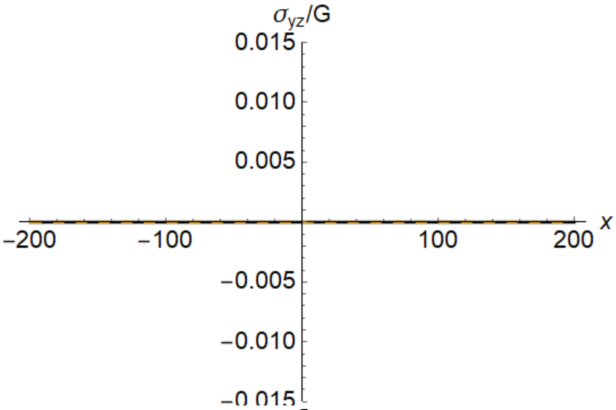

Fig. 6. Comparison of $\frac{\sigma_{yz}}{G}$ analytical solutions in this paper (solid and black line) to the results of DeVincre's Formula (dashed line) along *x*-direction for non-zero b_z

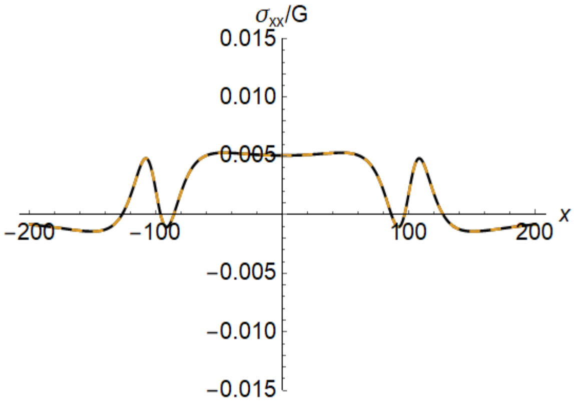

Fig. 7. Comparison of $\frac{\sigma_{xx}}{G}$ analytical solutions in this paper (solid and black line) to the results of DeVincre's Formula (dashed line) along *x*-direction for non-zero b_z

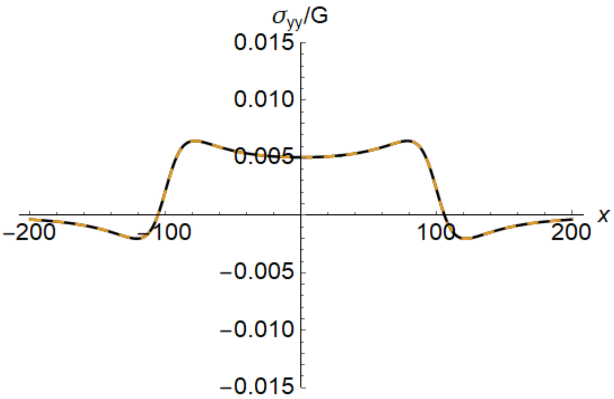

Fig. 8. Comparison of $\frac{\sigma_{yy}}{G}$ analytical solutions in this paper (solid and black line) to the results of DeVincre's Formula (dashed line) along *x*-direction for non-zero b_z

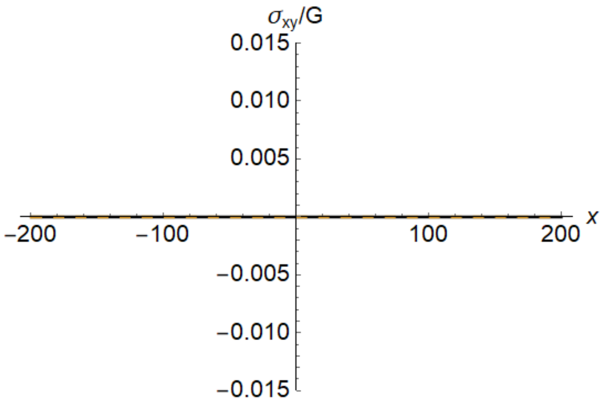

Fig. 9. Comparison of $\frac{\sigma_{xy}}{G}$ analytical solutions in this paper (solid and black line) to the results of DeVincre's Formula (dashed line) along *x*-direction for non-zero b_z

4. CONCLUSIONS

In conclusion, the stress field associated with a rectangular dislocation loop in an infinite medium has been developed. It is obtained by integrating the PK equation over a finite rectangular area. Also, the strain field can be developed by equation (11) if one is interested in it. The stress field obtained herein not only contributes to calculating the total stress fields of a rectangular dislocation loop in the isotropic half-medium, but also serves as a benchmarking tool for 3D dislocation dynamic codes which deal with generally-curved dislocations and need to properly quantify their elastic fields.

The developed field solutions were verified using both analytical equations and numerical calculations. The verifications were to ensure satisfaction of the equilibrium equations, satisfaction of the strain compatibility equations, and comparison against the stress field developed by DeVincre's Formula for straight dislocation segments.

5. LIMITATIONS

The main limitation of the current work is that it deals with isotropic and not anisotropic materials. It also deals with infinite and not finite domains.

ACKNOWLEDGEMENTS

Author LL would like to express gratitude for family support during his higher education.

COMPETING INTERESTS

Authors have declared that no competing interests exist.

REFERENCES

1. Meyers MA, Chawla KK. Mechanical Behavior of Materials. 2nd edition. University of Cambridge, UK; 2009.
2. Rhee M, Zbib HM, Hirth JP, Huang H, De La Rubia T. Modelling Simul Mater Sci Engng. 1998;6(4):467-492.
3. Zbib HM, Rhee M, Hirth JP, Int J Mech Sci. 1998;40(2-3):113-127.
4. Kubin LP, Canova G, Condat M, Devincre B, Pontikis V, and Brechet Y. Solid State Phenomena. 1992;23-24:455-472.
5. Devincre B. Solid St Commun. 1995; 93(11):875-878.
6. Hirth JP, Lothe J. Theory of Dislocations. 5th edition. Krieger Publishing Company, Malabar, Florida; 1982.
7. Hull D, Bacon DJ. Introduction to Dislocations. University of Liverpool, UK; 2011.
8. Weertman J, Weertman JR. Elementary Dislocation Theory. Oxford University Press, Oxford; 1992.
9. Kroupa F. Circular edge dislocation loop. Czech J Phys B. 1960;1:284–293.
10. Bullough R, Newman RC. The spacing of prismatic dislocation loops. Phil Mag. 1960;2:921–926.
11. Keller JM. 1957; unpublished
12. Kröner E. Kontinuumstheorie Der Versetzungen Und Eigenspannungen. Springer-Verlag, Berlin; 1958.
13. Kroupa F. Interaction between prismatic dislocation loops and straight dislocations Phil Mag. 1962;3:783–801.
14. Marcinkowski MJ, Sree Harsha KS. Properties of finite circular dislocation glide loops. J Appl Phys. 1968;4:1775–1783.
15. Khraishi TA, Hirth JP, Zbib HM, Khaleel MA. The displacement, and strain-stress fields of a general circular Volterra dislocation loop. International Journal of Engineering Science. 2000;5:251–266.
16. Khraishi TA, Zbib HM, Hirth JP, De La Rubia TD. The stress field of a general circular Volterra dislocation loop: analytical and numerical approaches. Phil Mag Lett. 2000;6:95–105.
17. Khraishi TA, Zbib HM. The displacement field of a rectangular Volterra dislocation loop. Phil Mag Lett. 2002;7:265–277.
18. Khraishi TA, Zbib HM, De La Rubia TD. The treatment of traction-free boundary condition in three-dimensional dislocation dynamics using generalized image stress analysis. Materials Science and Engineering A. 2001;309-310:283-287.
19. Khraishi TA, Zbib HM. Free surface effects in 3D dislocation dynamics: formulation and modeling. Journal of Engineering Materials and Technology (JEMT). 2002; 124(3):342-351.
20. Yan L, Khraishi TA, Shen Y-L, Horstemeyer MF. A distributed-dislocation method for treating free-surface image stresses in 3D dislocation Dynamics Simulations. Modelling and Simulation in Materials Science and Engineering. 2004; 12(4):S289-S301.
21. Siddique AB, Khraishi T. Numerical methodology for treating static and dynamic dislocation problems near a free surface. Journal of Physics Communications. 2020;4(5):055005. DOI 10.1088/2399-6528/ab8ff9
22. Khraishi TA, Zbib HM. Dislocation dynamics simulations of the interaction between a short rigid fiber and a glide circular dislocation pile-up. Computational Materials Science. 2002;24(3):310-322.
23. De La Rubia TD, Zbib HM, Khraishi TA, Wirth BD, Victoria M, Caturla MJ. Multiscale modelling of plastic flow localization in irradiated materials. Nature. 2000;406(6798):871-874.
24. Khraishi TA, Zbib HM, De La Rubia TD, Victoria M. Modeling of irradiation-induced hardening in metals using dislocation dynamics. Philosophical Magazine Letters. 2001;81(9):583-593.
25. Khraishi TA, Zbib HM, De La Rubia TD, Victoria M. Localized deformation and hardening in irradiated metals: Three-dimensional discrete dislocation dynamics simulations. Metallurgical and Materials Transactions B. 2002;33(2):285-296.
26. Demir I, Hirth JP, Zbib HM. Extended stress field around a cylindrical crack using the theory of dislocation pile-ups. International Journal of Engineering Science. 1992;8:829–845.
27. Demir I, Hirth JP, Zbib HM. The Somigliana ring dislocation. J Elasticity. 1992;9:223-246.
28. Demir I, Khraishi TA. The Torsional dislocation loop and mode III Cylindrical crack. Journal of Mechanics. 2005;10:115-122.

29. Gradshteyn IS, Ryzhik IM. Table of Integrals, Series, and Products. 5th edition. Academic Press: San Diego, California; 1980.
30. Khraishi TA, Shen, YL. Introductory Continuum Mechanics with Applications to Elasticity. University Readers/Cognella, San Diego, California; 2011.
31. Jesus Lerma, Tariq Khraishi, Sandeep Kataria, Yu-Lin Shen. Distributed dislocation method for determining elastic fields of 2D and 3D volume misfit particles in infinite space and extension of the method for particles in half space. Journal of Mechanics. 2015; 31(3):249-260.
32. Siddique AB, Khraishi TA. Eigenvalues and Eigenvectors for 3×3 Symmetric Matrices: An Analytical Approach, Journal of Advances in Mathematics and Computer Science. 2020;35(7):106-118. Available: https://doi.org/10.9734/jamcs/2020/v35i730308

APPENDIX

Considering the Burgers vector component b_x:

$$\frac{\sigma_{xx}}{G}=\frac{b_x p}{2B1K\pi}(\frac{Q3}{\sqrt{A2}}-\frac{Q4}{\sqrt{A1}})+\frac{b_x p}{2B2K\pi}(-\frac{Q3}{\sqrt{A4}}+\frac{Q4}{\sqrt{A3}})+\frac{b_x p}{4B1^2K\pi}(\frac{B1Q1^2Q3}{A2^{3/2}}-\frac{(p^2-Q1^2)Q3}{\sqrt{A2}}-\frac{B1Q1^2Q4}{A1^{3/2}}+\frac{(p^2-Q1^2)Q4}{\sqrt{A1}})+\frac{b_x p}{4B2^2K\pi}(-\frac{(B2Q2^2-A4(p^2-Q2^2))Q3}{A4^{3/2}}+\frac{(B2Q2^2-A3(p^2-Q2^2))Q4}{A3^{3/2}});$$

$$\frac{\sigma_{yy}}{G}=\frac{b_x p}{4\pi}(\frac{1}{K}(-\frac{Q3}{A2^{3/2}}+\frac{Q4}{A1^{3/2}})+\frac{2}{B1K}(\frac{Q3}{\sqrt{A2}}-\frac{Q4}{\sqrt{A1}})+\frac{1}{K}(\frac{Q3}{A4^{3/2}}-\frac{Q4}{A3^{3/2}})+\frac{2}{B2K}(-\frac{Q3}{\sqrt{A4}}+\frac{Q4}{\sqrt{A3}})+2(\frac{1}{B1}(\frac{Q3}{\sqrt{A2}}-\frac{Q4}{\sqrt{A1}})+\frac{1}{B2}(-\frac{Q3}{\sqrt{A4}}+\frac{Q4}{\sqrt{A3}})));$$

$$\frac{\sigma_{zz}}{G}=\frac{b_x p}{2B1K\pi}(\frac{Q3}{\sqrt{A2}}-\frac{Q4}{\sqrt{A1}})+\frac{b_x p}{2B2K\pi}(-\frac{Q3}{\sqrt{A4}}+\frac{Q4}{\sqrt{A3}})+\frac{b_x p}{4B1^2K\pi}(-\frac{(-B1p^2+A2(p^2+3Q1^2))Q3}{A2^{3/2}}+\frac{(-B1p^2+A1(p^2+3Q1^2))Q4}{A1^{3/2}})+\frac{b_x p}{4B2^2K\pi}(\frac{(-B2p^2+A4(p^2+3Q2^2))Q3}{A4^{3/2}}-\frac{(-B2p^2+A3(p^2+3Q2^2))Q4}{A3^{3/2}});$$

$$\frac{\sigma_{xy}}{G}=\frac{b_x p}{4K\pi}((-\frac{1}{A1^{3/2}}+\frac{1}{A2^{3/2}})Q1+(-\frac{1}{A3^{3/2}}+\frac{1}{A4^{3/2}})Q2)+\frac{b_x p}{4\pi}(\frac{1}{C2}(-\frac{Q1}{\sqrt{A1}}-\frac{Q2}{\sqrt{A3}})+\frac{1}{C1}(\frac{Q1}{\sqrt{A2}}+\frac{Q2}{\sqrt{A4}}));$$

$$\frac{\sigma_{xz}}{G}=\frac{b_x Q1}{4B1^2K\pi}(-(-\frac{B1p^2}{A2^{3/2}}-\frac{(p^2-Q1^2)}{\sqrt{A2}})Q3+(-\frac{B1p^2}{A1^{3/2}}-\frac{(p^2-Q1^2)}{\sqrt{A1}})Q4)+\frac{b_x}{4\pi}(\frac{1}{C1}(\frac{Q1}{\sqrt{A2}}+\frac{Q2}{\sqrt{A4}})Q3-\frac{1}{C2}(\frac{Q1}{\sqrt{A1}}+\frac{Q2}{\sqrt{A3}})Q4)+\frac{b_x Q2}{4B2^2K\pi}((\frac{B2p^2}{A4^{3/2}}+\frac{(p^2-Q2^2)}{\sqrt{A4}})Q3+(-\frac{B2p^2}{A3^{3/2}}-\frac{(p^2-Q2^2)}{\sqrt{A3}})Q4);$$

$$\frac{\sigma_{yz}}{G}=\frac{b_x}{4\pi}(\frac{1}{\sqrt{A1}}-\frac{1}{\sqrt{A2}}-\frac{1}{\sqrt{A3}}+\frac{1}{\sqrt{A4}}+\frac{1}{K}(-\frac{Q1^2+Q3^2}{A2^{3/2}}+\frac{Q2^2+Q3^2}{A4^{3/2}}+\frac{Q1^2+Q4^2}{A1^{3/2}}-\frac{Q2^2+Q4^2}{A3^{3/2}}));$$

Considering the Burgers vector component b_y:

$$\frac{\sigma_{xx}}{G}=\frac{b_y p}{4\pi}(2(\frac{1}{C2}(\frac{Q1}{\sqrt{A1}}+\frac{Q2}{\sqrt{A3}})+\frac{1}{C1}(-\frac{Q1}{\sqrt{A2}}-\frac{Q2}{\sqrt{A4}}))+\frac{1}{K}(-\frac{Q1}{A1^{3/2}}+\frac{Q1}{A2^{3/2}}-\frac{Q2}{A3^{3/2}}+\frac{Q2}{A4^{3/2}}+\frac{2}{C2}(\frac{Q1}{\sqrt{A1}}+\frac{Q2}{\sqrt{A3}})+\frac{2}{C1}(-\frac{Q1}{\sqrt{A2}}-\frac{Q2}{\sqrt{A4}})));$$

$$\frac{\sigma_{yy}}{G}=\frac{b_y p}{2C2K\pi}(\frac{Q1}{\sqrt{A1}}+\frac{Q2}{\sqrt{A3}})+\frac{b_y p}{2C1K\pi}(-\frac{Q1}{\sqrt{A2}}-\frac{Q2}{\sqrt{A4}})+\frac{b_y p}{4C1^2K\pi}(-\frac{C1Q1Q3^2}{A2^{3/2}}-\frac{C1Q2Q3^2}{A4^{3/2}}+\frac{Q1(p^2-Q3^2)}{\sqrt{A2}}+\frac{Q2(p^2-Q3^2)}{\sqrt{A4}})+\frac{b_y p}{4C2^2K\pi}(\frac{C2Q1Q4^2}{A1^{3/2}}+\frac{C2Q2Q4^2}{A3^{3/2}}-\frac{Q1(p^2-Q4^2)}{\sqrt{A1}}-\frac{Q2(p^2-Q4^2)}{\sqrt{A3}});$$

$$\frac{\sigma_{zz}}{G}=\frac{b_y p}{2C2K\pi}(\frac{Q1}{\sqrt{A1}}+\frac{Q2}{\sqrt{A3}})+\frac{b_y p}{2C1K\pi}(-\frac{Q1}{\sqrt{A2}}-\frac{Q2}{\sqrt{A4}})+\frac{b_y p}{4C1^2K\pi}(-\frac{C1p^2Q1}{A2^{3/2}}-\frac{C1p^2Q2}{A4^{3/2}}+\frac{Q1(p^2+3Q3^2)}{\sqrt{A2}}+\frac{Q2(p^2+3Q3^2)}{\sqrt{A4}})+\frac{b_y p}{4C2^2K\pi}(\frac{C2p^2Q1}{A1^{3/2}}+\frac{C2p^2Q2}{A3^{3/2}}-\frac{Q1(p^2+3Q4^2)}{\sqrt{A1}}-\frac{Q2(p^2+3Q4^2)}{\sqrt{A3}});$$

$$\frac{\sigma_{xy}}{G}=\frac{b_y p}{4K\pi}((-\frac{1}{A2^{3/2}}+\frac{1}{A4^{3/2}})Q3-(-\frac{1}{A1^{3/2}}+\frac{1}{A3^{3/2}})Q4)+\frac{b_y p}{4\pi}(\frac{1}{B1}(-\frac{Q3}{\sqrt{A2}}+\frac{Q4}{\sqrt{A1}})+\frac{1}{B2}(\frac{Q3}{\sqrt{A4}}-\frac{Q4}{\sqrt{A3}}));$$

$$\frac{\sigma_{xz}}{G}=\frac{b_y}{4\pi}(\frac{1}{\sqrt{A1}}-\frac{1}{\sqrt{A2}}-\frac{1}{\sqrt{A3}}+\frac{1}{\sqrt{A4}}+\frac{1}{K}(-\frac{Q1^2+Q3^2}{A2^{3/2}}+\frac{Q2^2+Q3^2}{A4^{3/2}}+\frac{Q1^2+Q4^2}{A1^{3/2}}-\frac{Q2^2+Q4^2}{A3^{3/2}}));$$

$$\frac{\sigma_{yz}}{G}=\frac{b_y Q3}{4C1^2K\pi}(\frac{C1p^2Q1}{A2^{3/2}}+\frac{C1p^2Q2}{A4^{3/2}}+\frac{Q1(p^2-Q3^2))}{\sqrt{A2}}+\frac{Q2(p^2-Q3^2)}{\sqrt{A4}})-\frac{b_y Q4}{4C2^2K\pi}(\frac{C2p^2Q1}{A1^{3/2}}+\frac{C2p^2Q2}{A3^{3/2}}+\frac{Q1(p^2-Q4^2)}{\sqrt{A1}}+\frac{Q2(p^2-Q4^2)}{\sqrt{A3}})+\frac{b_y}{4\pi}(\frac{Q1}{B1}(\frac{Q3}{\sqrt{A2}}-\frac{Q4}{\sqrt{A1}})+\frac{Q2}{B2}(\frac{Q3}{\sqrt{A4}}-\frac{Q4}{\sqrt{A3}}));$$

Considering the Burgers vector component b_z:

$$\frac{\sigma_{xx}}{G}=\frac{Q3b_z}{4K\pi}(\frac{Q1}{A2^{3/2}}+\frac{Q2}{A4^{3/2}})+\frac{Q3b_z}{2C1K\pi}(-\frac{Q1}{\sqrt{A2}}-\frac{Q2}{\sqrt{A4}})-\frac{Q4b_z}{4K\pi}(\frac{Q1}{A1^{3/2}}+\frac{Q2}{A3^{3/2}})-\frac{Q4b_z}{2C2K\pi}(-\frac{Q1}{\sqrt{A1}}-\frac{Q2}{\sqrt{A3}})$$
$$+\frac{Q1b_z}{2B1K\pi}(-\frac{Q3}{\sqrt{A2}}+\frac{Q4}{\sqrt{A1}})+\frac{Q2b_z}{2B2K\pi}(-\frac{Q3}{\sqrt{A4}}+\frac{Q4}{\sqrt{A3}})+\frac{b_z}{2\pi}(\frac{Q3}{C1}(-\frac{Q1}{\sqrt{A2}}-\frac{Q2}{\sqrt{A4}})$$
$$-\frac{Q4}{C2}(-\frac{Q1}{\sqrt{A1}}-\frac{Q2}{\sqrt{A3}}))+\frac{Q1b_z}{4B1^2K\pi}(-\frac{Q4(3B1p^2+(3p^2+Q1^2)(b-y)^2)}{A1^{3/2}}$$
$$+\frac{Q3(3B1p^2+(3p^2+Q1^2)(b+y)^2)}{A2^{3/2}})+\frac{Q2b_z}{4B2^2K\pi}(-\frac{Q4(3B2p^2+(3p^2+Q2^2)(b-y)^2)}{A3^{3/2}}$$
$$+\frac{Q3(3B2p^2+(3p^2+Q2^2)(b+y)^2)}{A4^{3/2}})$$

$$\frac{\sigma_{yy}}{G}=\frac{b_z}{4\pi}(\frac{2Q3}{C1K}(-\frac{Q1}{\sqrt{A2}}-\frac{Q2}{\sqrt{A4}})-\frac{2Q4}{C2K}(-\frac{Q1}{\sqrt{A1}}-\frac{Q2}{\sqrt{A3}})+\frac{Q1}{K}(\frac{Q3}{A2^{3/2}}-\frac{Q4}{A1^{3/2}})+\frac{2Q1}{B1K}(-\frac{Q3}{\sqrt{A2}}+\frac{Q4}{\sqrt{A1}})+$$
$$\frac{Q2}{K}(\frac{Q3}{A4^{3/2}}-\frac{Q4}{A3^{3/2}})+\frac{2Q2}{B2K}(-\frac{Q3}{\sqrt{A4}}+\frac{Q4}{\sqrt{A3}})+2(\frac{Q1}{B1}(-\frac{Q3}{\sqrt{A2}}+\frac{Q4}{\sqrt{A1}})+\frac{Q2}{B2}(-\frac{Q3}{\sqrt{A4}}+\frac{Q4}{\sqrt{A3}}))-$$
$$\frac{Q4}{C2^2K}(\frac{Q1(3p^4+a(3p^2+Q4^2)(a-2x)+(3p^2+x^2)(b-y)^2+3p^2x^2)}{A1^{3/2}}+$$
$$\frac{Q2(3p^4+a(3p^2+Q4^2)(a+2x)+(3p^2+x^2)(b-y)^2+3p^2x^2)}{A3^{3/2}})+$$
$$\frac{Q3}{C1^2K}(\frac{Q1(3p^4+a(3p^2+Q3^2)(a-2x)+(3p^2+x^2)(b+y)^2+3p^2x^2)}{A2^{3/2}}+\frac{Q2(3p^4+a(3p^2+Q3^2)(a+2x)+(3p^2+x^2)(b+y)^2+3p^2x^2)}{A4^{3/2}}));$$

$$\frac{\sigma_{zz}}{G}=\frac{Q3b_z}{2C1K\pi}(-\frac{Q1}{\sqrt{A2}}-\frac{Q2}{\sqrt{A4}})-\frac{Q4b_z}{2C2K\pi}(-\frac{Q1}{\sqrt{A1}}-\frac{Q2}{\sqrt{A3}})+\frac{Q1b_z}{2B1K\pi}(-\frac{Q3}{\sqrt{A2}}+\frac{Q4}{\sqrt{A1}})+\frac{Q2b_z}{2B2K\pi}(-\frac{Q3}{\sqrt{A4}}+\frac{Q4}{\sqrt{A3}})+$$
$$\frac{Q3b_z}{4C1^2(-\pi K)}(-\frac{-C1p^2Q1-A2Q1(p^2-Q3^2)}{A2^{3/2}}+\frac{C1p^2Q2+A4Q2(p^2-Q3^2)}{A4^{3/2}})-\frac{Q1b_z}{4B1^2(-\pi K)}(-\frac{B1p^2Q3+A2(p^2-Q1^2)Q3}{A2^{3/2}}+$$
$$\frac{B1p^2Q4+A1(p^2-Q1^2)Q4}{A1^{3/2}})+\frac{Q2b_z}{4B2^2(-\pi K)}(\frac{B2p^2Q3+A4(p^2-Q2^2)Q3}{A4^{3/2}}-\frac{B2p^2Q4+A3(p^2-Q2^2)Q4}{A3^{3/2}})+$$
$$\frac{Q4b_z}{4C2^2(-\pi K)}(\frac{-C2p^2Q1-A1Q1(p^2-Q4^2)}{A1^{3/2}}-\frac{Q2(p^4+p^2Q4^2+A3(p^2-Q4^2))}{A3^{3/2}})\ ;$$

$$\frac{\sigma_{xy}}{G}=\frac{b_z}{2\pi}(-\frac{1}{\sqrt{A1}}+\frac{1}{\sqrt{A2}}+\frac{1}{\sqrt{A3}}-\frac{1}{\sqrt{A4}})+\frac{b_z}{4K\pi}(\frac{B1}{A2^{3/2}}+\frac{B2}{A3^{3/2}}-\frac{B2}{A4^{3/2}}+\frac{C1}{A2^{3/2}}-\frac{C1}{A4^{3/2}}+\frac{C2}{A3^{3/2}}+\frac{-p^2-Q1^2}{A1^{3/2}}+$$
$$\frac{-p^2-Q4^2}{A1^{3/2}});$$

$$\frac{\sigma_{xz}}{G}=\frac{pQ3b_z}{4K\pi}(\frac{1}{A2^{3/2}}-\frac{1}{A4^{3/2}})+\frac{pb_z}{4K\pi}(-\frac{Q4}{A1^{3/2}}+\frac{Q4}{A3^{3/2}})+\frac{pb_z}{4B1^2K\pi}(-\frac{(p^2Q1^2+Q1^4-A2(p^2-Q1^2))Q3}{A2^{3/2}}+$$
$$\frac{(p^2Q1^2+Q1^4-A1(p^2-Q1^2))Q4}{A1^{3/2}})+\frac{pb_z}{4B2^2K\pi}(\frac{(B2Q2^2-A4(p^2-Q2^2))Q3}{A4^{3/2}}-\frac{(B2Q2^2-A3(p^2-Q2^2))Q4}{A3^{3/2}});$$

$$\frac{\sigma_{yz}}{G}=$$
$$\frac{b_z}{4K\pi}p((\frac{1}{A1^{3/2}}-\frac{1}{A2^{3/2}})Q1+(\frac{1}{A3^{3/2}}-\frac{1}{A4^{3/2}})Q2+\frac{1}{C1^2}(-\frac{Q1(-C1Q3^2+A2(p^2-Q3^2))}{A2^{3/2}}-$$
$$\frac{Q2(-C1Q3^2+A4(p^2-Q3^2))}{A4^{3/2}})+\frac{1}{C2^2}(\frac{Q1(A1(p^2-Q4^2)+Q4^2(-p^2-Q4^2))}{A1^{3/2}}+\frac{Q2(A3(p^2-Q4^2)+Q4^2(-p^2-Q4^2))}{A3^{3/2}}));$$

$p=c-z;$
$A1=p^2+(a-x)^2+(b-y)^2;$
$A2=p^2+(a-x)^2+(b+y)^2;$
$A3=p^2+(a+x)^2+(b-y)^2;$
$A4=p^2+(a+x)^2+(b+y)^2;$
$B1=p^2+(a-x)^2;$
$B2=p^2+(a+x)^2;$
$C1=p^2+(b+y)^2;$
$C2=p^2+(b-y)^2;$

$K = -1 + \nu;$
$\mathrm{Q1} = a - x;$
$\mathrm{Q2} = a + x;$
$\mathrm{Q3} = b + y;$
$\mathrm{Q4} = -b + y;$

Peer-review history:
The peer review history for this paper can be accessed here:
http://www.sdiarticle4.com/review-history/64597